Proportional-resonant controllers and filters for grid-connected voltage-source converters

R. Teodorescu, F. Blaabjerg, M. Liserre and P.C. Loh

Abstract: The recently introduced proportional-resonant (PR) controllers and filters, and their suitability for current/voltage control of grid-connected converters, are described. Using the PR controllers, the converter reference tracking performance can be enhanced and previously known shortcomings associated with conventional PI controllers can be alleviated. These shortcomings include steady-state errors in single-phase systems and the need for synchronous d–q transformation in three-phase systems. Based on similar control theory, PR filters can also be used for generating the harmonic command reference precisely in an active power filter, especially for single-phase systems, where d–q transformation theory is not directly applicable. Another advantage associated with the PR controllers and filters is the possibility of implementing selective harmonic compensation without requiring excessive computational resources. Given these advantages and the belief that PR control will find wide-ranging applications in grid-interfaced converters, PR control theory is revised in detail with a number of practical cases that have been implemented previously, described clearly to give a comprehensive reference on PR control and filtering.

1 Introduction

Over the years, power converters of various topologies have found wide application in numerous grid-interfaced systems, including distributed power generation with renewable energy sources (RES) like wind, hydro and solar energy, microgrid power conditioners and active power filters. Most of these systems include a grid-connected voltage-source converter whose functionality is to synchronise and transfer the variable produced power over to the grid. Another feature of the adopted converter is that it is usually pulse-width modulated (PWM) at a high switching frequency and is either current- or voltage-controlled using a selected linear or nonlinear control algorithm. The deciding criterion when selecting the appropriate control scheme usually involves an optimal tradeoff between cost, complexity and waveform quality needed for meeting (for example) new power quality standards for distributed generation in low-voltage grids, like IEEE-1547 in the USA and IEC61727 in Europe at a commercially favourable cost.

With the above-mentioned objective in view while evaluating previously reported control schemes, the general conclusion is that most controllers with precise reference tracking are either overburdened by complex computational

requirements or have high parametric sensitivity (sometimes both). On the other hand, simple linear proportional–integral (PI) controllers are prone to known drawbacks, including the presence of steady-state error in the stationary frame and the need to decouple phase dependency in three-phase systems although they are relatively easy to implement [1]. Exploring the simplicity of PI controllers and to improve their overall performance, many variations have been proposed in the literature including the addition of a grid voltage feedforward path, multiple-state feedback and increasing the proportional gain. Generally, these variations can expand the PI controller bandwidth but, unfortunately, they also push the systems towards their stability limits. Another disadvantage associated with the modified PI controllers is the possibility of distorting the line current caused by background harmonics introduced along the feedforward path if the grid voltage is distorted. This distortion can in turn trigger LC resonance especially when a LCL filter is used at the converter AC output for filtering switching current ripple [2, 3].

Alternatively, for three-phase systems, synchronous frame PI control with voltage feedforward can be used, but it usually requires multiple frame transformations, and can be difficult to implement using a low-cost fixed-point digital signal processor (DSP). Overcoming the computational burden and still achieving virtually similar frequency response characteristics as a synchronous frame PI controller, [4, 5], develops the P + resonant (PR) controller for reference tracking in the stationary frame. Interestingly, the same control structure can also be used for the precise control of a single-phase converter [5]. In brief, the basic functionality of the PR controller is to introduce an infinite gain at a selected resonant frequency for eliminating steady-state error at that frequency, and is therefore conceptually similar to an integrator whose infinite DC gain forces the DC steady-state error to zero. The resonant portion of the PR controller can therefore be viewed as a generalised AC integrator (GI), as proven in [6]. With the introduced

R. Teodorescu and F. Blaabjerg are with the Section of Power Electronics and Drives, Institute of Energy Technology, Aalborg University, Pontoppidanstraede 101, 9220 Aalborg East, Denmark

M. Liserre is with the Department of Electrotechnical and Electronic Engineering, Polytechnic of Bari, 70125-Bari, Italy

P.C. Loh is with the School of Electrical and Electronic Engineering, Nanyang Technological University, Nanyang Avenue, S639798, Singapore

E-mail: fbl@iet.aau.dk

750

IEE Proc.-Electr. Power Appl., Vol. 153, No. 5, September 2006

flexibility of tuning the resonant frequency, attempts at using multiple PR controllers for selectively compensating low-order harmonics have also been reported in [6, 7] for three-phase active power filters, in [8] for three-phase uninterruptible power supplies (UPS) and in [9] for single-phase photovoltaic (PV) inverters. Based on similar concept, various harmonic reference generators using PR filters have also been proposed for single-phase traction power conditioners [10] and three-phase active power filters [11].

From the view point that electronic power converters will find increasing grid-interfaced applications either as inverters processing DC energy from RES for grid injection or as rectifiers conditioning grid energy for different load usages, this paper aims to provide a comprehensive reference for readers on the integration of PR controllers and filters to grid-connected converters for enhancing their tracking performances. To begin, the paper reviews frequency-domain derivation of the ideal and non-ideal PR controllers and filters, and discusses their similarities as compared to classical PI control. Generic control block diagrams for illustrating current or voltage tracking control are next described before a number of practical cases that the authors have implemented previously are discussed to provide readers with some implementation examples. Throughout the presentation, experimental results are presented for validating the theoretical and implementation concepts discussed.

2 PR control and filtering derivation

The transfer functions of single- and three-phase PR controllers and filters can be derived using internal model control, modified state transformation or frequency-domain approach presented in [12, 13–15] and [4, 16], respectively. In this work, the latter approach is chosen for presentation as it clearly demonstrates similarities between PR controllers and filters in the stationary reference frame and their equivalence in the synchronous frame, as shown in the following Sections.

2.1 Derivation of single-phase PR transfer functions

For single-phase PI control, the popularly used synchronous d–q transformation cannot be applied directly, and the closest equivalence developed to date is to multiply the feedback error $e(t)$, in turn, by sine and cosine functions usually synchronised with the grid voltage using a phase-locked-loop (PLL), as shown in Fig. 1 [10, 17]. This achieves the same effect of transforming the component at the chosen frequency to DC, leaving all other components

Fig. 1 *Single-phase equivalent representations of PR and synchronous PI controllers*

as AC quantities. Take for example an error signal consisting of the fundamental and 3rd harmonic components, expressed as:

$$e(t) = E_1 \cos(\omega t + \theta_1) + E_3 \cos(3\omega t + \theta_3) \quad (1)$$

where ω, θ_1 and θ_3 represent the fundamental angular frequency, fundamental and third harmonic phase shifts respectively. Multiplying this with $\cos(\omega t)$ and $\sin(\omega t)$ gives, respectively:

$$e_C(t) = \frac{E_1}{2}\{\cos(\theta_1) + \cos(2\omega t + \theta_1)\}$$
$$+ \frac{E_3}{2}\{\cos(2\omega t + \theta_3) + \cos(4\omega t + \theta_3)\}$$
$$e_S(t) = \frac{E_1}{2}\{\sin(-\theta_1) + \sin(2\omega t + \theta_1)\}$$
$$+ \frac{E_3}{2}\{\sin(-2\omega t - \theta_3) + \sin(4\omega t + \theta_3)\} \quad (2)$$

It is observed that the fundamental term now appears as DC quantities $\cos(\theta_1)$ and $\sin(-\theta_1)$. The only complication with this equivalent single-phase conversion is that the chosen frequency component not only appears as a DC quantity in the synchronous frame, it also contributes to harmonic terms at a frequency of 2ω (this is unlike three-phase synchronous d–q conversion where the chosen frequency component contributes only towards the DC term). Nevertheless, passing $e_c(t)$ and $e_s(t)$ through integral blocks would still force the fundamental error amplitude E_1 to zero, caused by the infinite gain of the integral blocks.

Instead of transforming the feedback error to the equivalent synchronous frame for processing, an alternative approach of transforming the controller $G_{DC}(s)$ from the synchronous to the stationary frame is also possible. This frequency-modulated process can be mathematically expressed as:

$$G_{AC}(s) = G_{DC}(s - j\omega) + G_{DC}(s + j\omega) \quad (3)$$

where $G_{AC}(s)$ represents the equivalent stationary frame transfer function [10]. Therefore, for the ideal and non-ideal integrators of $G_{DC}(s) = K_i/s$ and $G_{DC}(s) = K_i/(1 + (s/\omega_c))$ (K_i and $\omega_c \ll \omega$ represent controller gain and cutoff frequency respectively), the derived generalised AC integrators $G_{AC}(s)$ are expressed as:

$$G_{AC}(s) = \frac{Y(s)}{E(s)} = \frac{2K_i s}{s^2 + \omega^2} \quad (4)$$

$$G_{AC}(s) = \frac{Y(s)}{E(s)} = \frac{2K_i(\omega_c s + \omega_c^2)}{s^2 + 2\omega_c s + (\omega_c^2 + \omega^2)}$$
$$\approx \frac{2K_i \omega_c s}{s^2 + 2\omega_c s + \omega^2} \quad (5)$$

Equation (4), when grouped with a proportional term K_p, gives the ideal PR controller with an infinite gain at the AC frequency of ω (see Fig. 2a), and no phase shift and gain at other frequencies. For K_p, it is tuned in the same way as for a PI controller, and it basically determines the dynamics of the system in terms of bandwidth, phase and gain margin. To avoid stability problems associated with an infinite gain, (5) can be used instead of (4) to give a non-ideal PR controller and, as illustrated in Fig. 2b, its gain is now finite, but still relatively high for enforcing small steady-state error. Another feature of (5) is that, unlike (4), its bandwidth can be widened by setting ω_c appropriately, which can be helpful for reducing sensitivity towards (for example) slight frequency variation in a typical utility grid (for (4), K_i can be tuned for shifting the magnitude response vertically, but
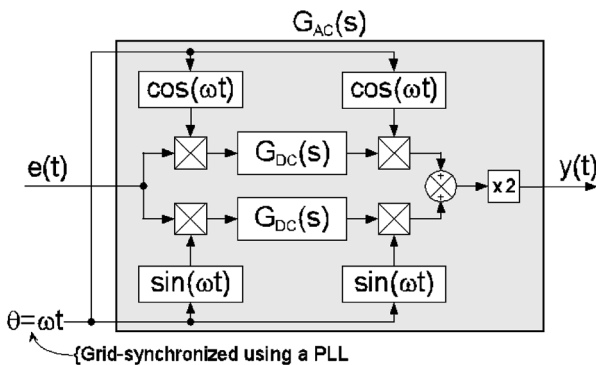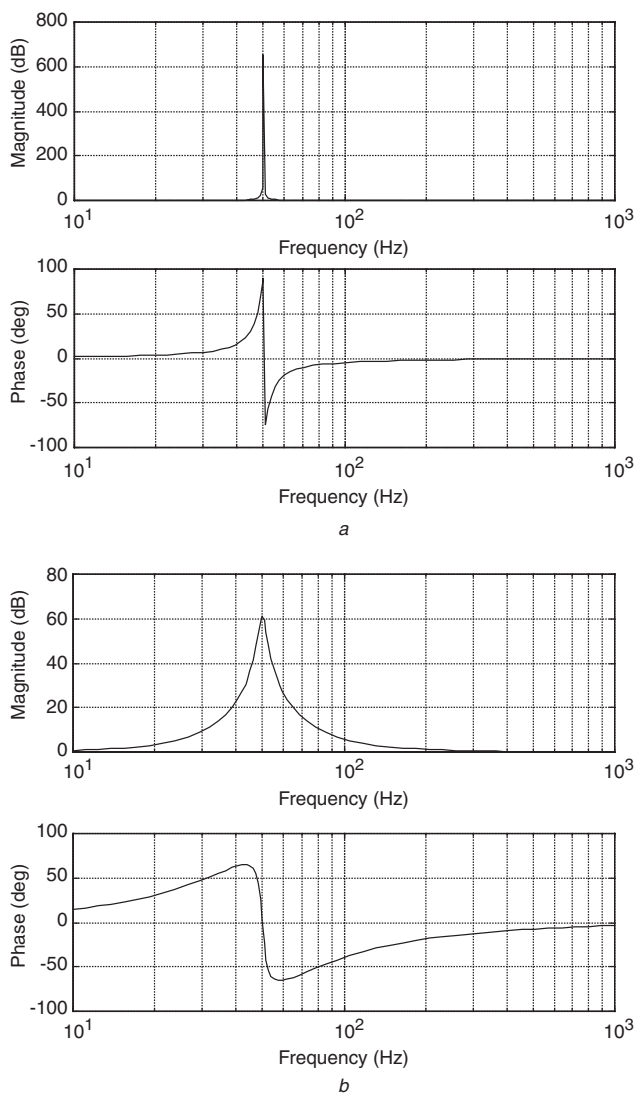
Fig. 2 *Bode plots of ideal and non-ideal PR compensators*
$K_P = 1$, $K_i = 20$, $\omega = 314$ rad/s and $\omega_c = 10$ rad/s
a Ideal
b Non-ideal

this does not give rise to a significant variation in bandwidth). In passing, note that a third control structure of $G_{AC}(s) = 2K_i\omega/(s^2 + \omega^2)$, can similarly be used since according to the internal model principle, it introduces a mathematical model that can generate the required sinusoidal reference along the open-loop control path, and therefore can ensure overall zero steady-state error [12]. This third form is, however, not preferred since the absence of a zero at $s = 0$ causes its response to be relatively slower [12].

Besides single frequency compensation, selective harmonic compensation can also be achieved by cascading several resonant blocks tuned to resonate at the desired low-order harmonic frequencies to be compensated for. As an example, the transfer functions of an ideal and a non-ideal harmonic compensator (HC) designed to compensate for the 3rd, 5th and 7th harmonics (as they are the most prominent harmonics in a typical current spectrum) are given as:

$$G_h(s) = \sum_{h=3,5,7} \frac{2K_{ih}s}{s^2 + (h\omega)^2} \qquad (6)$$

$$G_h(s) = \sum_{h=3,5,7} \frac{2K_{ih}\omega_c s}{s^2 + 2\omega_c s + (h\omega)^2} \qquad (7)$$

where h is the harmonic order to be compensated for and K_{ih} represents the individual resonant gain, which must be tuned relatively high (but within stability limit) for minimising the steady-state error. An interesting feature of the HC is that it does not affect the dynamics of the fundamental PR controller, as it compensates only for frequencies that are very close to the selected resonant frequencies.

Because of this selectiveness, (7) with K_{ih} set to unity, implying that each resonant block now has a unity resonant peak, can also be used for generating harmonic command reference in an active filter. The generic block representation is given in Fig. 3*a*, where the distorted load current (or voltage) is sensed and fed to the resonant filter $G_h(s)$, whose frequency response is shown in Fig. 3*b* for two different values of ω_c, $\omega = 2\pi \times 50$ rad/s and $h = 3, 5, 7$. Obviously, Fig. 3*b* shows the presence of unity (or 0 dB) resonant peaks at only the selected filtering frequencies of 150, 250 and 350 Hz for extracting the selected harmonics as command reference for the inner current loop. Also noted in the Figure is that as, ω_c gets smaller, $G_h(s)$ becomes more selective (narrower resonant peaks). However, using a smaller ω_c will make the filter more sensitive to frequency variations, lead to a slower transient response and make the filter implementation on a low-cost 16-bit DSP more difficult owing to coefficient quantisation and round-off errors. In practice, ω_c values of 5–15 rad/s have been found to provide a good compromise [10].

2.2 Derivation of three-phase PR transfer functions

For three-phase systems, elimination of steady-state tracking error is usually performed by first transforming the feedback variable to the synchronous d–q reference frame before applying PI control. Using this approach, double computational effort must be devoted under unbalanced conditions, during which transformations to both the positive- and negative-sequence reference frames are
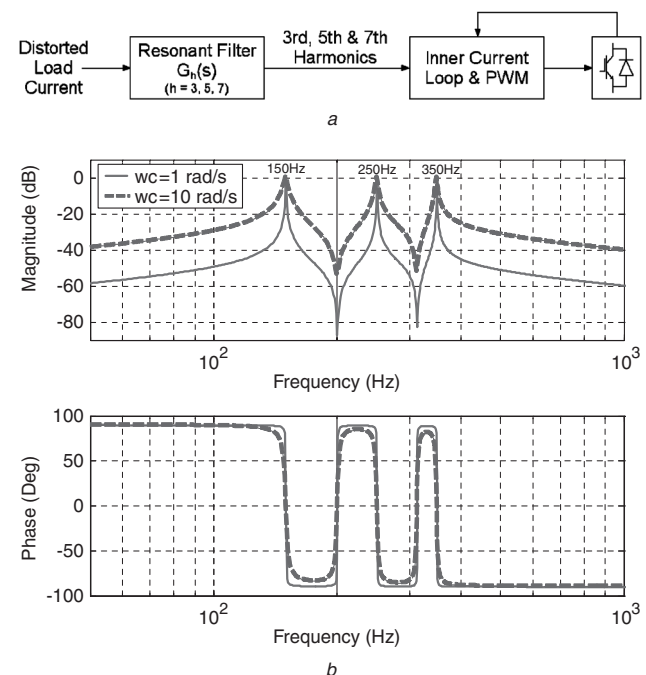
Fig. 3 *Resonant filter for filtering 3rd, 5th and 7th harmonics*
$K_{ih} = 1$, $\omega_c = 1$ rad/s and 10 rad/s
a Block representation
b Bode plots

required (see Fig. 4). An alternative simpler method of implementation is therefore desired and can be derived by inverse transformation of the synchronous controller back to the stationary α-β frame $G_{dq}(s) \rightarrow G_{\alpha\beta}(s)$. The inverse transformation can be performed by using the following 2×2 matrix:

$$G_{\alpha\beta}(s) = \frac{1}{2}\begin{bmatrix} G_{dq1} + G_{dq2} & jG_{dq1} - jG_{dq2} \\ -jG_{dq1} + jG_{dq2} & G_{dq1} + G_{dq2} \end{bmatrix}$$
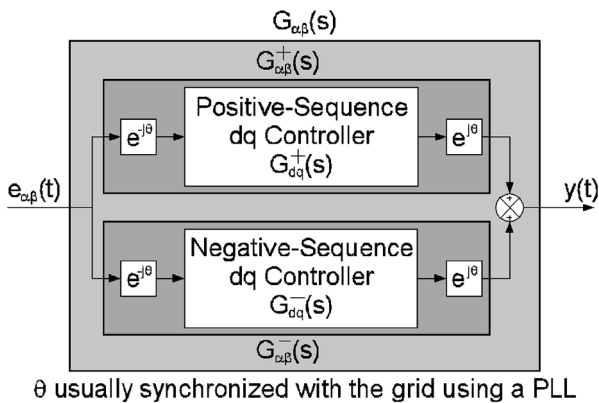
$$G_{dq1} = G_{dq}(s + j\omega)$$

$$G_{dq2} = G_{dq}(s - j\omega)$$

(8)

Given that $G_{dq}(s) = K_i/s$ and $G_{dq}(s) = K_i/(1 + (s/\omega_c))$, the equivalent controllers in the stationary frame for compensating for positive-sequence feedback error are therefore expressed as:

$$G_{\alpha\beta}^+(s) = \frac{1}{2}\begin{bmatrix} \dfrac{2K_i s}{s^2 + \omega^2} & \dfrac{2K_i\omega}{s^2 + \omega^2} \\ -\dfrac{2K_i\omega}{s^2 + \omega^2} & \dfrac{2K_i s}{s^2 + \omega^2} \end{bmatrix}$$

(9)

$$G_{\alpha\beta}^+(s) \simeq \frac{1}{2}\begin{bmatrix} \dfrac{2K_i\omega_c s}{s^2 + 2\omega_c s + \omega^2} & \dfrac{2K_i\omega_c\omega}{s^2 + 2\omega_c s + \omega^2} \\ -\dfrac{2K_i\omega_c\omega}{s^2 + 2\omega_c s + \omega^2} & \dfrac{2K_i\omega_c s}{s^2 + 2\omega_c s + \omega^2} \end{bmatrix}$$

(10)

Fig. 4 *Three-phase equivalent representations of PR and synchronous PI controllers considering both positive- and negative-sequence components*

Similarly, for compensating for negative sequence feedback error, the required transfer functions are expressed as:

$$G_{\alpha\beta}^-(s) = \frac{1}{2}\begin{bmatrix} \dfrac{2K_i s}{s^2 + \omega^2} & -\dfrac{2K_i\omega}{s^2 + \omega^2} \\ \dfrac{2K_i\omega}{s^2 + \omega^2} & \dfrac{2K_i s}{s^2 + \omega^2} \end{bmatrix}$$

(11)

$$G_{\alpha\beta}^-(s) \simeq \frac{1}{2}\begin{bmatrix} \dfrac{2K_i\omega_c s}{s^2 + 2\omega_c s + \omega^2} & -\dfrac{2K_i\omega_c\omega}{s^2 + 2\omega_c s + \omega^2} \\ \dfrac{2K_i\omega_c\omega}{s^2 + 2\omega_c s + \omega^2} & \dfrac{2K_i\omega_c s}{s^2 + 2\omega_c s + \omega^2} \end{bmatrix}$$

(12)

Comparing (9) and (10) with (11) and (12), it is noted that the diagonal terms of $G_{\alpha\beta}^+(s)$ and $G_{\alpha\beta}^-(s)$ are identical, but their non-diagonal terms are opposite in polarity. This inversion of polarity can be viewed as equivalent to the reversal of rotating direction between the positive- and negative-sequence synchronous frames.

Combining the above equations, the resulting controllers for compensating for both positive- and negative-sequence feedback errors are expressed as:

$$G_{\alpha\beta}(s) = \frac{1}{2}\begin{bmatrix} \dfrac{2K_i s}{s^2 + \omega^2} & 0 \\ 0 & \dfrac{2K_i s}{s^2 + \omega^2} \end{bmatrix}$$

(13)

$$G_{\alpha\beta}(s) \simeq \frac{1}{2}\begin{bmatrix} \dfrac{2K_i\omega_c s}{s^2 + 2\omega_c s + \omega^2} & 0 \\ 0 & \dfrac{2K_i\omega_c s}{s^2 + 2\omega_c s + \omega^2} \end{bmatrix}$$

(14)

Bode plots representing (13) and (14) are shown in Fig. 5, where their error-eliminating ability is clearly reflected by the presence of two resonant peaks at the positive frequency ω and negative frequency $-\omega$. Note that, if (9) or (10) ((11) or (12)) is used instead, only the resonant peak at ω ($-\omega$) is present since those equations represent PI control only in the positive-sequence (negative-sequence) synchronous frame. Another feature of (13) and (14) is that they have no cross-coupling non-diagonal terms, implying that each of the α and β stationary axes can be treated as a single-phase system. Therefore, the theoretical knowledge described earlier for single-phase PR control is equally applicable to the three-phase functions expressed in (13) and (14).
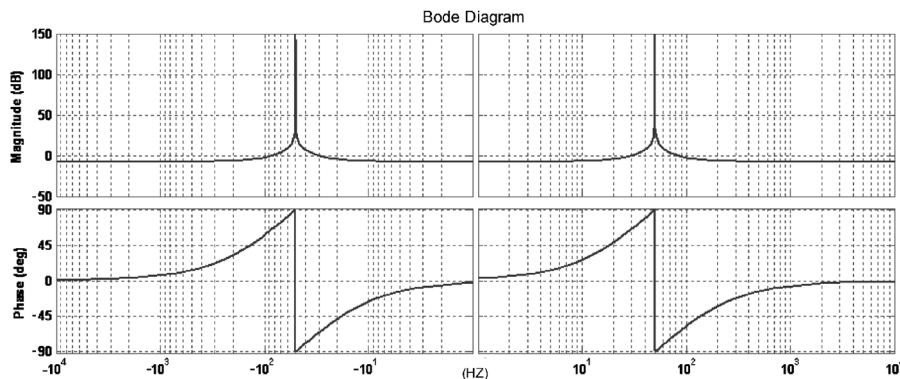
Fig. 5 *Positive- and negative-sequence Bode diagrams of PR controller*

IEE Proc.-Electr. Power Appl., Vol. 153, No. 5, September 2006

753

3 Implementation of resonant controllers

The resonant transfer functions in (4) and (5) (similarly in (13) and (14)) can be implemented using analogue integrated circuits (IC) or a digital signal processor (DSP), with the latter being more popular. Because of this, two methods of digitising the controllers are presented in detail after a general description of the analogue approach is given.

3.1 Analogue implementation
The rational function in (4) can be rewritten as [9]:

$$\frac{Y(s)}{E(s)} = \frac{2K_i s}{s^2 + \omega^2} \Rightarrow \left\{ Y(s) = \frac{1}{s}[2K_i E(s) - V_2(s)] \quad V_2(s) = \frac{1}{s}\omega^2 Y(s) \right.$$
(15)

Similarly, the function in (5) can be rewritten as:

$$\frac{Y(s)}{E(s)} = \frac{2K_i \omega_c s}{s^2 + 2\omega_c s + \omega^2}$$

$$\Rightarrow \begin{cases} Y(s) = \frac{1}{s}[2K_i\omega_c E(s) - V_1(s) - V_2(s)] \\ V_1(s) = 2\omega_c Y(s) \\ V_2(s) = \frac{1}{s}\omega^2 Y(s) \end{cases}$$
(16)

Equations (15) and (16) can both be represented by the control block representation shown in Fig. 6, where the upper feedback path is removed for representing (15). From this Figure, it can be deduced that the resonant function can be physically implemented using op-amp integrators and inverting/non-inverting gain amplifiers. Note also that, while implementing (15), parasitic resistance and other second-order imperfections would cause it to degenerate into (16), but of course its bandwidth can only be tuned if additional components are added for implementing the upper feedback path.

3.2 Shift-operator digital implementation
The most commonly used digitisation technique is the pre-warped bilinear (Tustin) transform [18], given by:

$$s = \frac{\omega_1}{\tan(\omega_1 T/2)}\frac{z-1}{z+1} = K_T \frac{z-1}{z+1}$$
(17)

where ω_1 is the pre-warped frequency, T is the sampling period and z is the forward shift operator. Equation (17) can then be substituted into (5) ((4) is not considered here owing to possible stability problems associated with its infinite resonant gain [4, 5]) for obtaining the z-domain discrete transfer function given in (18), from which the difference equation needed for DSP implementation is
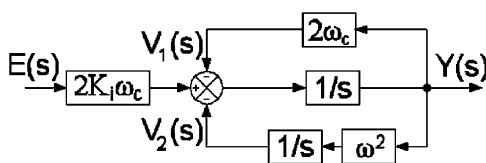
derived and expressed in (19) (where n represents the point of sampling):

$$\frac{Y(z)}{E(z)} = \frac{a_1 z^{-1} - a_2 z^{-2}}{b_0 - b_1 z^{-1} + b_2 z^{-2}}$$

$$a_1 = a_2 = 2K_i K_T \omega_c$$

$$b_0 = K_T^2 + 2K_T \omega_c + \omega^2$$

$$b_1 = 2K_T^2 - 2\omega^2$$

$$b_2 = \begin{cases} K_T^2 + 2K_T\omega_c + \omega^2 \\ K_T^2 + 2K_T\omega_c + (h\omega)^2 \quad \text{for } h = 3, 5, 7 \end{cases}$$
(18)

$$y(n) = \frac{1}{b_0}\{a_1[e(n-1) - e(n-2)] + b_1 y(n-1) - b_2 y(n-2)\}$$
(19)

Equations (18) and (19) can similarly be used for implementing the HC compensator after the desired harmonic order h is substituted. The resulting difference equation can conveniently be programmed into a floating-point DSP, but when a fixed-point DSP is used instead, coefficients of (19) have to be normalised by multiplying them with the maximum integer value of the chosen word length [10, 19]. This multiplication is needed for minimising the extent of coefficient quantisation error, and the choice of word length is solely dictated by the size of error that can be tolerated (large coefficient quantisation error should be avoided since it can change the frequency characteristics of a resonant peak, and even render it 'open-loop' unstable). Unfortunately, no standard method of choosing this word length is available and, as discussed in [10, 19], the appropriate word length is usually determined experimentally with the aim of achieving the best tradeoff between execution speed and accuracy.

3.3 δ-operator digital implementation
Generally, when the shift-operator resonant implementation given in (18) and (19) is programmed into a fixed-point DSP, some performance degradations can usually be observed and are caused mainly by round-off errors associated with the use of integer variables on the fixed-point DSP (so-called finite word length effect). 16-bit fixed-point implementation always has finite word length effects, but the problem is particularly pronounced at a fast sampling rate and for sharply tuned filters such as the resonant function used for PR control. Specifically, the roundoff errors cause the voltage or current wave shape to change slightly from cycle to cycle, resulting in significant fluctuations in its RMS value, as proven in [10].

To improve the resonant precision, the use of delta operator δ in place of the conventional shift operator has been investigated. The delta operator has recently gained importance in fast digital control owing to its superior finite word length performance [19–22], and it can be defined in terms of the shift operator z as:

$$\delta^{-1} = \frac{\Delta z^{-1}}{1 - z^{-1}}$$
(20)

Essentially, delta-operator resonant implementation involves converting a second-order section in z into a

Fig. 6 *Decomposition of resonant block into two interlinked integrators*

corresponding second-order Section in δ, as follows:

$$H(z) = \frac{b_0 + b_1 z^{-1} + b_2 z^{-2}}{1 + a_1 z^{-1} + a_2 z^{-2}}$$

$$\Rightarrow H(\delta) = \frac{\beta_0 + \beta_1 \delta^{-1} + \beta_2 \delta^{-2}}{1 + \alpha_1 \delta^{-1} + \alpha_2 \delta^{-2}} \qquad (21)$$

where $\beta_0 = b_0$, $\beta_1 = (2b_0 + b_1)/\Delta$, $\beta_2 = (b_0 + b_1 + b_2)/\Delta^2$, $\alpha_0 = 1$, $\alpha_1 = (2 + a_1)/\Delta$, $\alpha_2 = (1 + a_1 + a_2)/\Delta^2$, and Δ is a positive constant less than unity, which is carefully chosen to select the appropriate ranges for the α and β coefficients, and to minimise other internal variable truncation noise [22]. Equation (21) is then implemented using the transposed direct form II (DFIIt) structure shown in Fig. 7. The DFIIt structure is chosen out of the many filter structures available because it has the best roundoff noise performance for delta-operator-based filters [22]. From Fig. 7, the difference equations to be coded for the DSP can be written, in processing order, as:

$$w_4(n) = \Delta w_3(n-1) + w_4(n-1)$$
$$w_2(n) = \Delta w_1(n-1) + w_2(n-1)$$
$$y(n) = \beta_0 x(n) + w_4(n) \qquad (22)$$
$$w_3(n) = \beta_1 x(n) - \alpha_1 y(n) + w_2(n)$$
$$w_5(n) = \beta_2 x(n) - \alpha_2 y(n)$$

Note that the first two equations in (22) for $w_4(n)$ and $w_2(n)$ are obtained from the definition of the delta operator given in (20). In addition, similar to (19), the coefficients in (22) will initially be floating-point numbers and must be normalised by multiplying them with the maximum integer
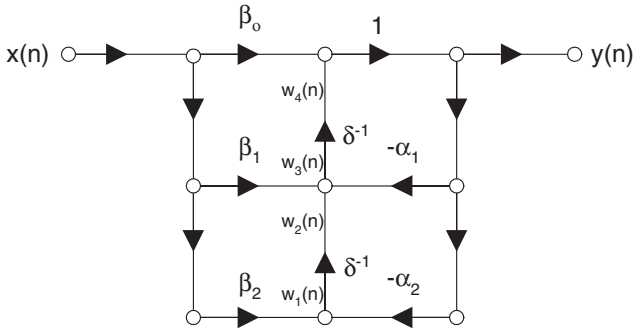
Fig. 7 *Direct form II transpose (DFIIt) structure for second-order digital filter*
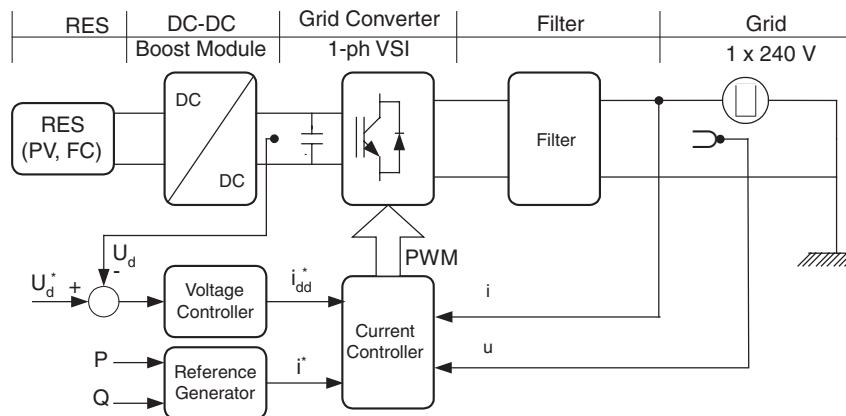
value of the chosen word length for faster and accurate execution in a fixed-point DSP. This required word length and the constant Δ together represent two degrees of design freedom that can be used for optimising the round-off performance against coefficient quantisation and potential overflows, often through experimental testing.
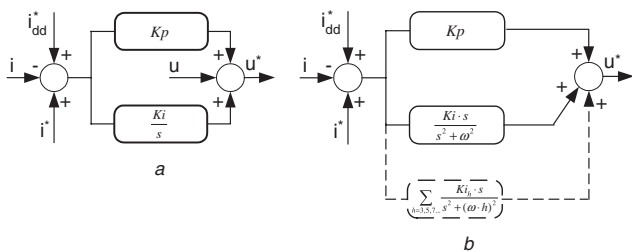
4 Example cases using PR controllers or filters

Given the advantages of PR controllers and filters, a number of applications have since been proposed in the literature with most focusing on the control of converters interfaced directly to the utility grid. In this Section, two example cases are presented for demonstrating the effectiveness of using PR controllers in a single-phase PV converter [9], and a three-phase microgrid power quality compensator [14].

4.1 Single-phase PV grid-connected inverter

Single-phase grid inverters are commonly used in applications like residential RES (typically PV or fuel cell systems) and UPS. Figure 8 shows a typical RES where the DC-link voltage, active P and reactive Q power are controlled in the outer control loops (labelled as voltage controller and reference generator in the Figure). The reference current outputs of the outer loops (i^*_{dd} and i^*) are next tracked by an inner current loop whose output is eventually fed to a PWM modulator for switching the inverter.

Typically, the inner current loop is implemented using a stationary PI current controller with voltage feedforward, as shown in Fig. 9a. Using PI control, however, leads to steady-state current error (both in phase and magnitude) when tracking sinusoidal input, and hence a poor harmonic compensation performance is expected [9]. Synchronous PI control described in Section 2.1 can mitigate the tracking error, but is generally difficult to apply. Instead, the equivalent stationary PR controller can be used as the inner current controller, as shown in Fig. 9b. Compared to a stationary PI controller, the only computational requirement imposed by the PR controller is an extra integrator for implementing a second-order system, but with a modern low-cost 16-bit fixed-point DSP, this increase in computation can generally be ignored [9]. Besides that, using a PR controller would allow the removal of the grid voltage feedforward path, as proven in [9], and the simple cascading of a HC compensator for eliminating selected low-order harmonics.


Fig. 8 *Block diagram of typical single-phase RES system*

IEE Proc.-Electr. Power Appl., Vol. 153, No. 5, September 2006

755

Fig. 9 *Single-phase grid inverter control*
a Stationary PI control
*b* Stationary PR inner current control

The designed control scheme in Fig. 9*b* has been tested using an experimental 3 kW PV full-bridge inverter with an output LCL filter, as shown in Fig. 10. The inverter is powered from a regulated DC power supply (set to $U_D = 350$ V) for simulating a PV string, and is interfaced to the utility grid with a voltage of $U_g = 230$ V RMS and a background THD of 1.46%. The resulting system is controlled digitally using a 16-bit fixed-point TMS320F24xx DSP platform with an execution time of 40 μs (including HC compensation) and the controller gains set as $K_p = 2$, $K_i = 300$ and $K_{ih} = 300$ for $h = 3$, 5 and 7. With these settings, the grid current and voltage at 50% load using PR and PR + HC controllers are shown in Figs. 11 and 12 respectively. As seen in Fig. 11, there is no phase error noted between the grid current and voltage, confirming the proper functioning of the PR controller. The harmonic distortion in Fig. 11 can be further reduced by cascading an HC compensator, as demonstrated by the smoother current waveform in Fig. 12.
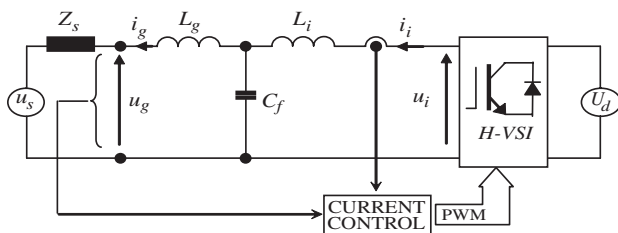
Fig. 10 *Schematic representation of experimental single-phase PV inverter*
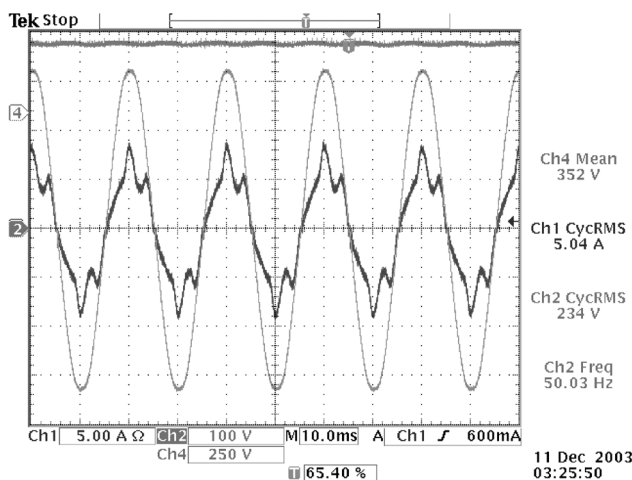
Fig. 11 *Waveforms captured using PR controller at 50% load*
Grid voltage Ch2 [100 V/div.], grid current Ch1 [5 A/div.] and DC voltage Ch4 [250 V/div.]
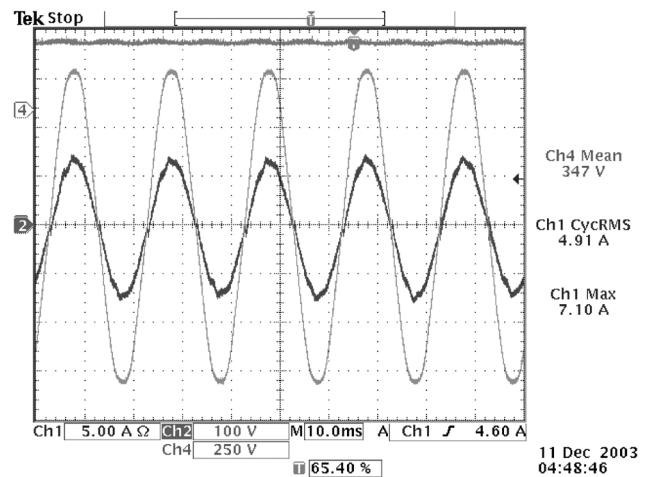
**Fig. 12** *Waveforms captured using PR+HC controller at 50% load*
Grid voltage Ch2 [100 V/div.], grid current Ch1 [5 A/div.] and DC voltage Ch4 [250 V/div.]

The improved performance achieved here with a single-phase inverter can obviously be extended to a three-phase RES (e.g. small wind or water turbines and high-power PV plant) since as explained in Section 2.2, three-phase control in the stationary α–β frame can be viewed as two independent control paths along the α and β axes, respectively. For illustration, Fig. 13*b* shows the inner current control scheme of a three-phase RES inverter, where a second PR controller is added, as compared to that in Fig. 9*b*. Also shown in Fig. 13*a* is the conventional synchronous PI method of implementation, where multiple frame transformations and control decoupling are needed. These complications are obviously removed from Fig. 13*b* when PR controllers are used instead.

4.2 Three-phase microgrid power quality compensator

In Section 4.1, the precise current tracking and selective harmonic compensation functionalities of the PR controllers in a single-phase inverter have been demonstrated. This Section now presents a second example on a microgrid power quality compensator for demonstrating that the PR controllers can equally be used in a voltage control loop and can simultaneously compensate for both positive- and negative-sequence components.

In general, microgrids can be viewed as 'local area networks' where clusters of micro-generators are installed for distributed power generation. For interfacing these microsystems to the utility grid, while simultaneously refining the waveform quality at the point of coupling (PCC), a microgrid power quality compensator, consisting of a shunt and a series inverter (labelled as inverters A and B, respectively), can be used [14], as shown in Fig. 14. In principle, shunt inverter A is controlled to maintain a balanced set of three-phase voltages in the microgrid under all grid and load operating conditions. Besides voltage regulation, inverter A is also tasked to perform other functions such as the proper dispatch of active and reactive power, and the synchronisation of the micro- and utility grids during the transition from islanding to grid-connected mode [14], but these are not described here since the focus of this paper is mainly on the application of PR controllers for voltage or current tracking. On the other hand, series inverter B is controlled to inject appropriate voltage components along the distribution feeder for blocking large

756

IEE Proc.-Electr. Power Appl., Vol. 153, No. 5, September 2006
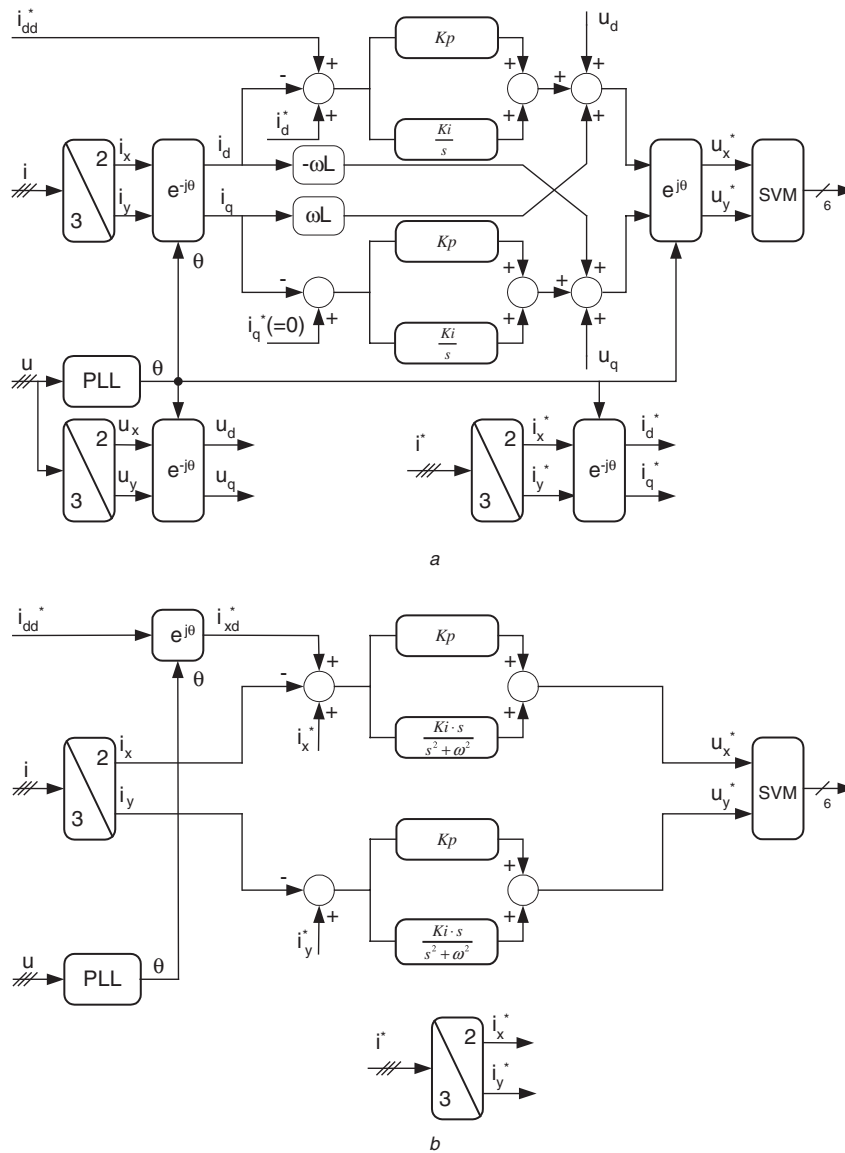
Fig. 13 *Three-phase grid inverter current control*
a Using Synchronous PI controller
b Using PR controllers
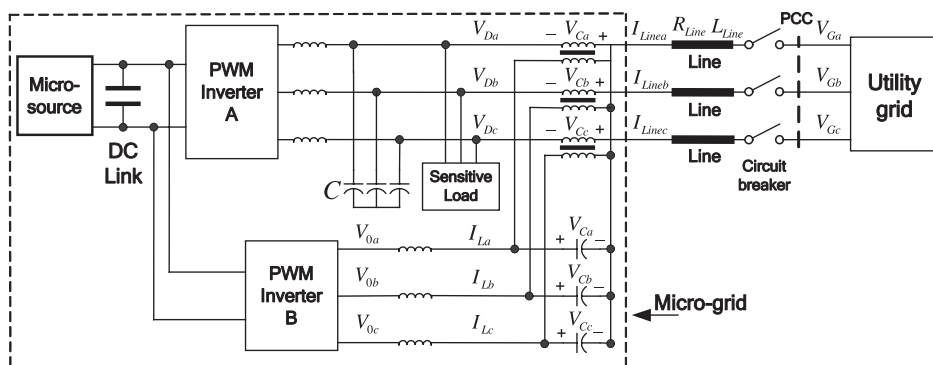
Fig. 14 *Schematic of microgrid interfaced to utility grid using power quality compensator*

negative-sequence currents that might flow along the low-impedance line if the PCC voltages are unbalanced.

With the assigned control tasks in view, Fig. 15 shows the control block representation of shunt inverter A, where the measured inverter voltage phasor $V_{\alpha\beta}(s)$ is forced to track its reference $V_{\alpha\beta}^*(s)$ precisely using the PR control block

$G_{\alpha\beta}(s)$. The generated output is then fed to an inner proportional current regulator for providing a faster dynamic response. (In passing, it is commented that the same control structure can be used for controlling a UPS and a dynamic voltage restorer (DVR), as presented in [23] and [24], respectively.) Similarly, the control block diagram
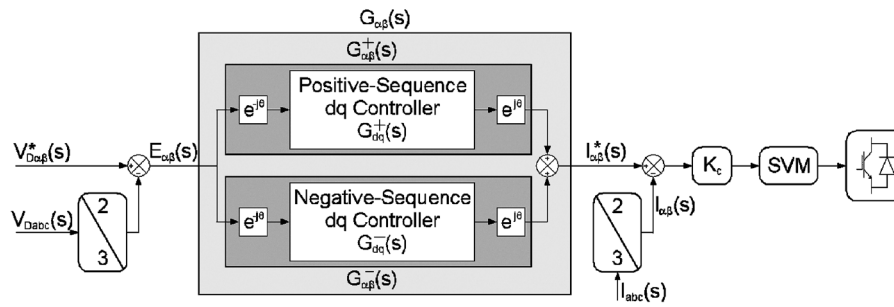
IEE Proc.-Electr. Power Appl., Vol. 153, No. 5, September 2006

757

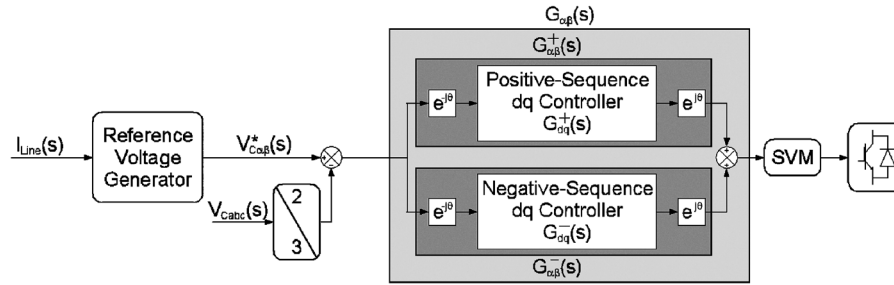**Fig. 15** *Voltage control scheme of shunt inverter A*

Fig. 16 *Control scheme of series inverter B for compensating negative-sequence current*

of series inverter B is shown in Fig. 16, where the line current phasor $I_{Line}(s)$ is measured and used for generating the required negative-sequence voltage command $V^*_{C\alpha\beta}(s)$ needed for forcing the negative-sequence line current to zero. This command reference is then closely tracked by the measured inverter voltage phasor $V_{C\alpha\beta}(s)$, again using a PR control block $G_{\alpha\beta}(s)$. Note that an inner current loop for enhancing the dynamic response of inverter B is deemed unnecessary since the line current response is primarily limited by the feeder line impedance.

For verifying the tracking performance of the PR controllers in the inverter control schemes, a hardware prototype has been built in the laboratory using the system parameters listed in Table 1. For the experimental system, a programmable AC source is used to represent the utility grid and is connected to an emulated microgrid. The microgrid consists of shunt inverter A, series inverter B with

Table 1: Parameters of implemented microgrid power compensator

Parameter	Value
Nominal line-to-line grid voltage	120 V
Frequency	50 Hz
DC supply voltage	250 V
Switching frequency for both inverters	10 kHz
Series inverter filter capacitance	10 µF
Series inverter filter inductance	3.9 mH
Series transformer turns ratio	1 : 1
Shunt inverter filter capacitance	30 µF
Shunt inverter filter inductance	5 mH
Line resistance R_{Line}	3 Ω
Line inductance L_{Line}	10 mH
Grid dispatch power	300 W, 160 var
Sensitive load in the microgrid	120 W, 90 var

an injection transformer and a connected RL load. Both inverters are controlled using a single dSPACE DS1103 processor card with the slave TMS320F240 processor on the card configured to perform carrier-based PWM.

Under grid-connected mode of operation, Figs. 17*a* and *b* show the utility voltages and microgrid load voltages, respectively, where the utility voltages become unbalanced with 0.1 p.u. negative-sequence and 0.1 p.u. zero-sequence voltage components added at $t = 3.8$ s. Despite this unbalance in utility voltages, the load voltages in the microgrid are kept balanced by controlling shunt inverter A. Similarly, by controlling series inverter B, the currents flowing between the microgrid and utility grid can be balanced. This is demonstrated in Fig. 18, where the captured line current waveforms are converted to the negative-sequence synchronous frame (post-processing in Matlab) for a better illustration of how the DC negative-sequence current components vary. As anticipated, the negative-sequence *d*–*q* components gradually decrease to zero, implying the proper functioning of series inverter B.

## 5 Other recent areas of development

Besides being used as PR controllers and filters, the frequency-domain resonant concept has also been used in a number of related control developments. These developments are summarised herein to give an insight into some perspective applications of the resonant concept.

5.1 Highpass equivalent stationary frame filter
In a three-phase active power filter, it is a common practice to transform the measured load current to the (positive-sequence) synchronous reference frame before extracting the harmonic components using a highpass filter [11, 25]. The extracted harmonics are then used as command reference for the active filter inner current loop, as shown in Fig. 19. Using a similar concept as in Section 2.2, the highpass filter block, expressed as $G^+_{dq}(s) = s/(s + \omega_c)$, can
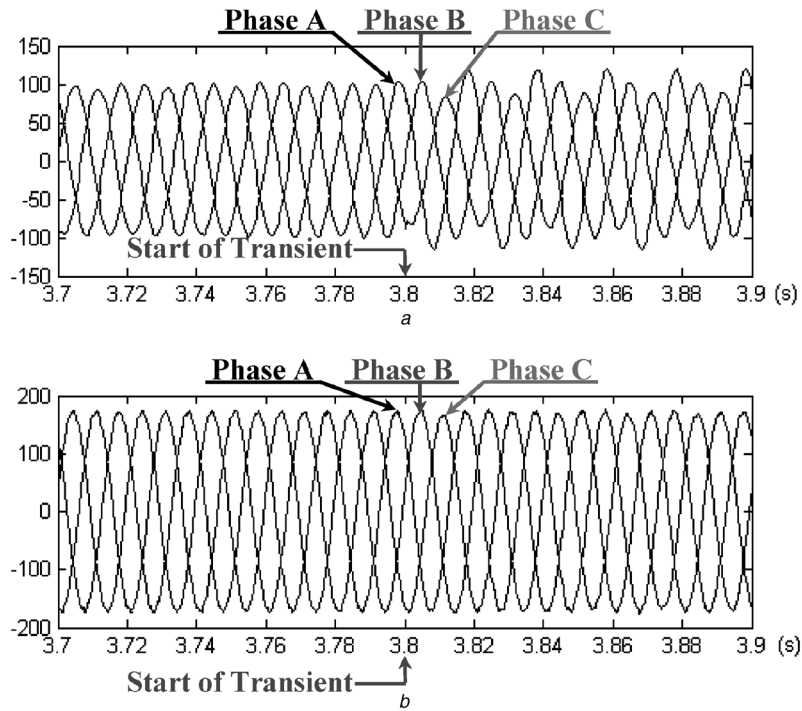
Fig. 17 *Experimental utility grid voltages and sensitive load voltages in microgrid*
a Utility grid voltages
b Sensitive load voltages
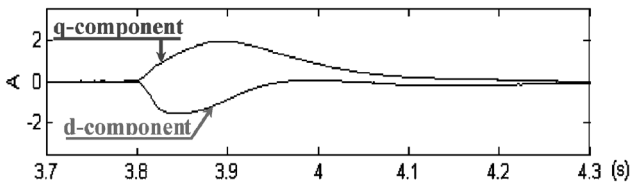
Fig. 18 *Experimental line currents in the negative-sequence synchronous d–q frame*
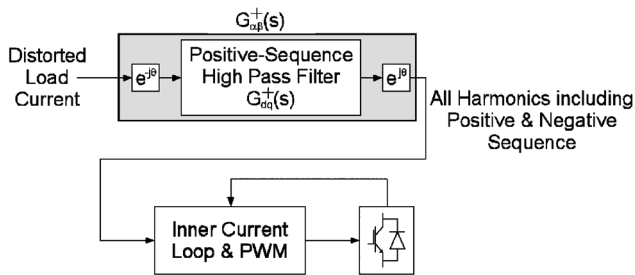
Fig. 19 *Block representation of typical active filter control scheme*

be inverse-transformed to the stationary α–β frame, and is expressed as [11]:

$$G_{\alpha\beta}^+(s) = \begin{bmatrix} \dfrac{s^2 + \omega_c s + \omega^2}{s^2 + 2\omega_c s + \omega_c^2 + \omega^2} & \dfrac{-\omega_c \omega}{s^2 + 2\omega_c s + \omega_c^2 + \omega^2} \\[3mm] \dfrac{\omega_c \omega}{s^2 + 2\omega_c s + \omega_c^2 + \omega^2} & \dfrac{s^2 + \omega_c s + \omega^2}{s^2 + 2\omega_c s + \omega_c^2 + \omega^2} \end{bmatrix}$$

(23)

Since (23) is directly derived from the highpass filter in the positive-sequence synchronous frame, it is expected to filter out all positive- and negative-sequence harmonics from the distorted load current for compensation. The source current supplied by the grid would therefore consist only of a positive-sequence fundamental component assuming that the inner current loop of the active filter is implemented with high tracking precision.

5.2 Hybrid repetitive control

In [26–30], two alternative repetitive control schemes are presented, whose control block representations are shown in Figs. 20*a* and *b*. Empirically, the control schemes can be viewed as the cascaded connection of a delayed feedback path and a feedforward path that resemble classical repetitive [31, 32] and Posicast control [33–35], respectively. With the cascading of these two classical control theories, it is interesting that it is shown in [26–28] that the control scheme in Fig. 20*a* can be expressed as (24), while the
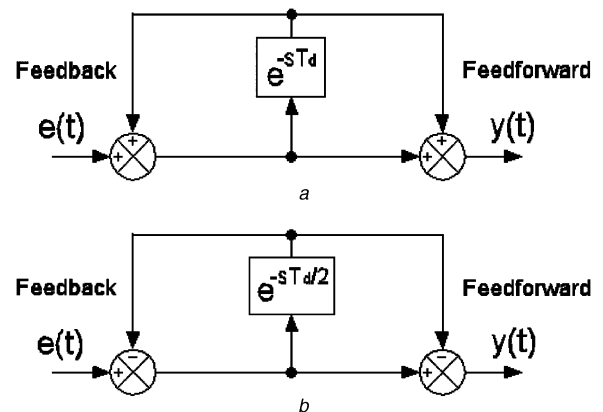
Fig. 20 *Block representations of hybrid repetitive and Posicast control*
a Positive feedback and feedforward
b Negative feedback and feedforward

IEE Proc.-Electr. Power Appl., Vol. 153, No. 5, September 2006

759

scheme in Fig. 20b can be expressed as (25):

$$\frac{Y(s)}{E(s)} = \frac{1 + e^{-sT_d}}{1 - e^{-sT_d}} = \frac{2}{T_d}\left\{ \frac{1}{s} + \sum_{h=1}^{\infty} \frac{2s}{s^2 + (h\omega)^2} \right\} \quad (24)$$

$$\frac{Y(s)}{E(s)} = \frac{1 - e^{-sT_d/2}}{1 + e^{-sT_d/2}} = \frac{4}{T_d}\left\{ \sum_{k=1}^{\infty} \frac{2s}{s^2 + [(2k-1)\omega]^2} \right\} \quad (25)$$

Obviously, (24) and (25) feature multiple harmonic resonant compensators for eliminating all harmonics in (24) and odd harmonics in (25). This extent of harmonic compensation would be computationally intensive if multiple resonant compensators in (4) or (5) are used, but with the schemes presented in Fig. 20, only a single time delay block is needed. These hybrid repetitive schemes are therefore attractive alternatives with promising application in grid converters.

Besides the schemes described above, another hybrid repetitive scheme with a degree of control freedom for selecting the desired harmonics to be compensated for is proposed in [36]. The proposed controller is recommended for discrete-time implementation using a DSP, and is shown schematically in Fig. 21. Compared with a traditional positive feedback repetitive controller, the controller described in [36] has an additional 'discrete-Fourier-transform (DFT)' filter block $F_{DFT}(z)$ inserted along the forward path, which is mathematically expressed as:

$$F_{DFT}(z) = \sum_{h \in N_h} F_{dh}(z) = \sum_{h \in N_h} \left(\frac{2}{N} \sum_{i=0}^{N-1} \cos\left[\frac{2\pi}{N} h(i + N_a) \right] z^{-i} \right)$$

$$= \frac{2}{N} \sum_{i=0}^{N-1} \left(\sum_{h \in N_h} \cos\left[\frac{2\pi}{N} h(i + N_a) \right] \right) z^{-i} = \frac{2}{N} \sum_{i=0}^{N-1} \vartheta_i z^{-i} \quad (26)$$

where i, N, h and N_h represent the ith sample point, number of samples within a fundamental period, harmonic order and set of harmonics selected for compensation respectively. Equation (26) also includes an additional term N_a for introducing a defined number of leading steps (equivalent to a leading phase shift), which, when used with the feedback z^{-Na} block, stabilises the system against phase delays, rounding and quantisation errors introduced by the digital sampling process.

For showing that the DFT scheme approximates the HC compensator in (6), the transfer functions of both schemes should be re-expressed as (assuming $N_a = 0$ for the DFT scheme):

DFT repetitive

$$G_{DFT}(z) = \frac{Y(z)}{E(z)} = K_F \frac{\sum_{h \in N_h} F_{dh}(z)}{1 - \sum_{h \in N_h} F_{dh}(z)} \quad (27)$$
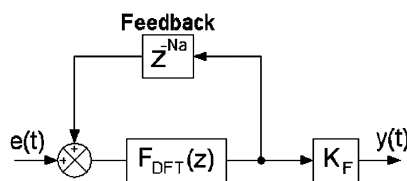
Fig. 21 *Block representation of repetitive control with selective harmonic compensation*

Resonant HC

$$G_h(s) = \frac{Y(s)}{E(s)} = K_{HC} \sum_{h \in N_h} \frac{F_h(s)}{1 - F_h(s)} \simeq K_{HC} \frac{\sum_{h \in N_h} F_h(s)}{1 - \sum_{h \in N_h} F_h(s)}$$

$$F_h(s) = \frac{2\xi_h h\omega s}{s^2 + 2\xi_h h\omega s + (h\omega)^2}; \quad K_{HC} = \frac{K_{ih}}{\xi_h h\omega} \quad (28)$$

where K_F and K_{HC} are gain constants, and ξ_h is the arbitrary damping factor of bandpass filter $F_h(s)$ (note that the approximation in (28) is always valid when multiple (very selective) bandpass filters are cascaded together [36]). Comparing (27) and (28), and noting that both $F_{dh}(z)$ and $F_h(s)$ have bandpass characteristics, the DFT repetitive scheme reported in [36] is virtually equivalent to the resonant HC compensator. However, observing (26), an identified feature of the DFT scheme is that its computational complexity does not worsen as the number of harmonics to be compensated for increases. Instead, the increase in harmonic number can simply be adapted by changing coefficient ϑ_i in (26). The DFT scheme is therefore a recommended choice for digital implementation, especially when a fixed-point DSP is used.

5.3 Synchronous frame selective harmonic compensation

In [37], a synchronous frame HC scheme is proposed for three-phase systems, where multiple resonant compensators are again used for eliminating selected harmonics. The sole difference here is that compensation is performed in the positive-sequence synchronous frame rotated at the fundamental frequency, where all $(6k \pm 1)\omega$ harmonics in the stationary frame are transformed to $\pm 6k\omega$ positive- and negative-sequence components in the rotated frame. The number of resonant compensators needed in the synchronous frame is therefore one-half those in its stationary frame counterpart since, as noted in Section 2.2, the resonant functions in (13) and (14) can simultaneously compensate for opposite rotating sequence components. This method of implementation is thus highly suitable for use when the number of harmonics to be compensated for is high. A further development of the idea of using a harmonic controller in a synchronous frame has been proposed in [38], where a frame rotating at a generic speed is considered, and the advantages and limits of the approach are discussed.

5.4 Resonant phase-locked-loop

In [37], the application of a resonant filter in a standard PLL is also explored. As shown in Fig. 22a, the measured grid voltage V_g is assumed to be distorted and an orthogonal system generation block is used to extract the fundamental voltages V_α and V_β. The orthogonal generation block consists of a resonant filter whose feedforward path produces an undistorted sinusoidal signal V_α, while its inner feedback path produces a second sinusoidal signal V_β phase-shifted by $90°$ (see Fig. 22b). The filtered voltages V_α and V_β are then fed to a standard PLL, whose input block first converts V_α and V_β to the synchronous d–q frame. In the synchronous frame, the d-axis component V_d is forced to zero by a PI controller, whose output is added to a nominal frequency value ω_{ff} to give the commanded angular frequency of ω^*. ω^* is next integrated to give an angle $\hat{\theta}$ synchronised with the utility grid (this angle is used in [37] for implementing the synchronous frame
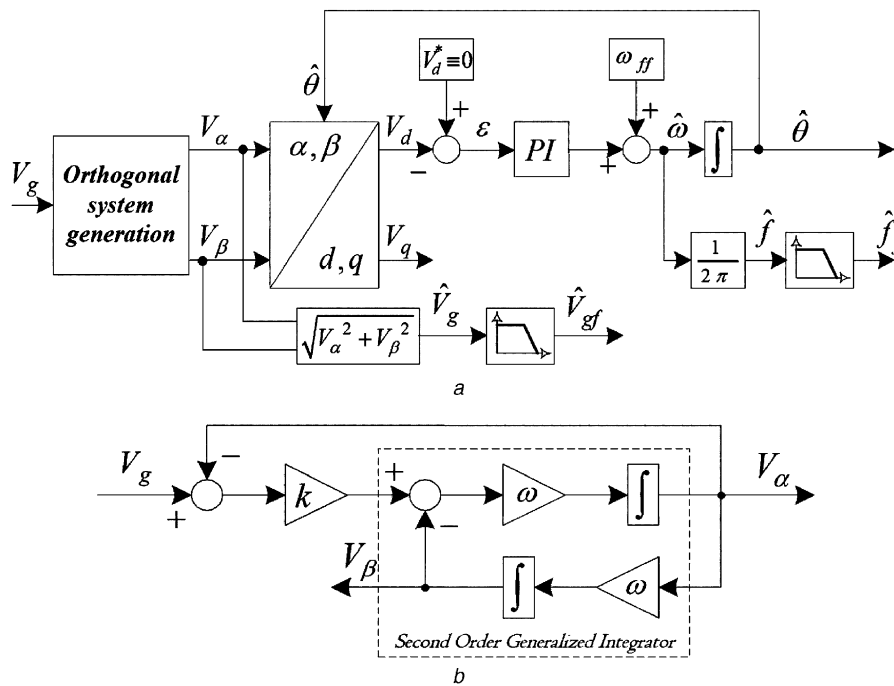
Fig. 22 *Block representation of PLL using a resonant filter*
a General structure
b Orthogonal system generation structure

compensator presented in Section 5.3). Besides $\hat{\theta}$, the grid frequency and voltage amplitude can also be estimated by performing simple mathematical manipulations, which are also shown in Fig. 22*a*.

6 Conclusions

In this paper, single- and three-phase PR control schemes have been reviewed and their implementation options and suitability for current/voltage control of grid-interfaced converters evaluated. Advantages of the PR controllers include the possibility of tuning their individual resonant peaks to the grid frequency for precise fundamental reference tracking and to some low-order harmonic frequencies for selective harmonic compensation, and the possibility of implementing harmonic reference generator in the stationary frame needed for active filters. Implementation wise, the PR technique requires lesser computational overhead and does not require an explicit grid voltage feedforward control path, while still achieving the same performance as a synchronous PI controller. For three-phase systems, the PR technique also has the unique feature of compensating for both positive- and negative-sequence components simultaneously, unlike synchronous PI where separate frame transformations are needed. Given these advantages, it is in the view of the authors that PR controllers can certainly replace their PI counterparts. This view has been supported by some recent developments summarised in the paper for a comprehensive review on PR control.

7 References

1 Kazmierkowski, M., Krishnan, R., and Blaabjerg, F.: 'Control in power electronics. Selected problems' (Academic Press, 2002)
2 Teodorescu, R., Blaabjerg, F., Liserre, M., and Dell'Aquila, A.: 'A stable three-phase LCL-filter based active rectifier without damping'. Proc. IEEE-IAS, Salt Lake City, UT, USA, 2003, pp. 1552–1557
3 Liserre, M., Blaabjerg, F., and Hansen, S.: 'Design and control of an LCL-filter based active rectifier', *IEEE Trans. Ind. Appl.*, 2001, **38**, pp. 299–307
4 Zmood, D.N., Holmes, D.G., and Bode, G.: 'Frequency domain analysis of three-phase linear current regulator', *IEEE Trans. Ind. Appl.*, 2001, **37**, pp. 601–610
5 Zmood, D.N., and Holmes, D.G.: 'Stationary frame current regulation of PWM inverters with zero steady-state error', *IEEE Trans. Power Electron.*, 2003, **18**, pp. 814–822
6 Yuan, X., Merk, W., Stemmler, H., and Allmeling, J.: 'Stationary-frame generalized integrators for current control of active power filters with zero steady-state error for current harmonics of concern under unbalanced and distorted operating conditions', *IEEE Trans. Ind. Appl.*, 2002, **38**, pp. 523–532
7 Mattavelli, P.: 'A closed-loop selective harmonic compensation for active filters', *IEEE Trans. Ind. Appl.*, 2001, **37**, pp. 81–89
8 Mattavelli, P.: 'Synchronous-frame harmonic control for high-performance AC power supplies', *IEEE Trans. Ind. Appl.*, 2001, **37**, pp. 864–872
9 Teodorescu, R., Blaabjerg, F., Liserre, M., and Borup, U.: 'A new control structure for grid-connected PV inverters with zero steady-state error and selective harmonic compensation'. Proc. IEEE, APEC4, Anaheim, CA, USA, 2004, pp. 580–586
10 Tan, P.C., Loh, P.C., and Holmes, D.G.: 'High performance harmonic extraction algorithm for a 25 kV traction power conditioner', *IEE Proc., Electr. Power Appl.*, 2004, **151**, pp. 505–512
11 Newman, M.J., Zmood, D.N., and Holmes, D.G.: 'Stationary frame harmonic reference generation for active power filter systems', *IEEE Trans. Ind. Appl.*, 2002, **38**, pp. 1591–1599
12 Fukuda, S., and Yoda, T.: 'A novel current-tracking method for active filters based on a sinusoidal internal model', *IEEE Trans. Ind. Appl.*, 2001, **37**, pp. 888–895
13 Jacobina, C.B., Correa, M.B. DER., Oliveiro, T.M., Lima, A.M.N., and da Silva, E.R.C.: 'Current control of unbalanced electrical systems', *IEEE Trans. Ind. Electron.*, 2001, **48**, pp. 517–525
14 Li, Y.W., Vilathgamuwa, D.M., and Loh, P.C.: 'A grid-interfacing power quality compensator for three-phase three-wire microgrid applications', *IEEE Trans. Power Electron.*, 2006, (to be published)
15 Li, Y.W., Vilathgamuwa, D.M., and Loh, P.C.: 'Micro-grid power quality enhancement using a three-phase four-wire grid-interfacing compensator', *IEEE Trans. Ind. Appl.*, 2005, **41**, pp. 1707–1719
16 D'Azzo, J.J., and Houpis, C.H.: 'Feedback control system analysis and synthesis' (McGraw-Hill, USA, 1966, 2nd edn.)
17 Tnani, S., Mazaudier, M., Berthon, A., and Diop, S.: 'Comparison between differential real-time harmonic analysis methods for control of electrical machines'. Proc. PEVSD, London, UK, 1994, pp. 342–345
18 Franklin, G.F., Powell, J.D., and Workman, M.: 'Digital control of dynamic systems' (Addison Wesley Longman Inc, 1998, 3rd edn.)
19 Newman, M.J., and Holmes, D.G.: 'Delta operator digital filters for high performance inverter applications', *IEEE Trans. Power Electron.*, 2003, **18**, pp. 447–454
20 Sera, D., Kerekes, T., Lungeanu, M., Nakhost, P., Teodorescu, R., Andersen, G.K., and Liserre, M.: 'Low-cost implementation of proportional-resonant current controllers for PV inverter applications

IEE Proc.-Electr. Power Appl., Vol. 153, No. 5, September 2006

761

using delta operator'. Proc. IEEE IECON, Raleigh, NC, USA, 2005, pp. 2517–2522

21 Middleton, R.H., and Goodwin, G.C.: 'Improved finite word length characteristics in digital control using delta operators', *IEEE Trans. Autom. Control*, 1986, **AC-31**, pp. 1015–1021

22 Kauraniemi, J., Laakso, T.I., Hartimo, I., and Ovaska, S.J.: 'Delta operator realizations of direct-form IIR filters', *IEEE Trans. Circuits Syst. II-Analog Dig. Signal Process.*, 1998, **45**, pp. 41–52

23 Loh, P.C., Newman, M.J., Zmood, D.N., and Holmes, D.G.: 'A comparative analysis of multi-loop voltage regulation strategies for single and three-phase UPS systems', *IEEE Trans. Power Electron.*, 2003, **18**, pp. 1176–1185

24 Loh, P.C., Vilathgamuwa, D.M., Tang, S.K., and Long, H.L.: 'Multilevel dynamic voltage restorer', *IEEE Power Electron. Lett.*, 2004, **2**, pp. 125–130

25 Fujita, H., and Akagi, H.: 'Unified power quality conditioner: the integration of series and shunt-active filters', *IEEE Trans. Power Electron.*, 1998, **13**, pp. 315–322

26 Escobar, G., Valdez, A.A., Leyva-Ramos, J., and Mattavelli, P.: 'A repetitive-based controller for UPS using a combined capacitor/load current sensing'. Proc. IEEE-PESC, Recife, Brazil, 2005, pp. 955–961

27 Escobar, G., Martinez, P.R., Leyva-Ramos, J., Valdez, A.A., and Hernandez-Gomez, M.: 'A repetitive-based controller for a power factor precompensator with harmonic compensation'. Proc. IEEE-PESC, Recife, Brazil, 2005, pp. 2363–2369

28 Escobar, G., Leyva-Ramos, J., Martinez, P.R., and Valdez, A.A.: 'A repetitive-based controller for the boost converter to compensate the harmonic distortion of the output voltage', *IEEE Trans. Control Syst. Tech.*, 2005, **13**, pp. 500–508

29 Leyva-Ramos, J., Escobar, G., Martinez, P.R., and Mattavelli, P.: 'Analog circuits to implement repetitive controllers for tracking and disturbance rejection of periodic signals', *IEEE Trans. Circuits Syst. II*, 2005, **52**, pp. 466–470

30 Escobar, G., Ortega, R., Astolfi, A., Martinez, M.F., and Leyva-Ramos, J.: 'A repetitive based controller for a shunt active filter to compensate for reactive power and harmonic distortion'. Proc. 44th IEEE Conf. on Decision and Control and European Control Conf. (ECC), Seville, Spain, 2005, pp. 6480–6485

31 Tzou, Y.Y., Ou, R.S., Jung, S.L., and Chang, M.Y.: 'High-performance programmable AC power source with low harmonic distortion using DSP-based repetitive control technique', *IEEE Trans. Power Electron.*, 1997, **12**, pp. 715–725

32 Costa-Castello, R., Grino, R., and Fossas, E.: 'Odd-harmonic digital repetitive control of a single-phase current active filter', *IEEE Trans. Power Electron.*, 2004, **19**, pp. 1060–1068

33 Smith, O.J.M.: 'Posicast control of damped oscillatory systems', *Proc. IRE*, 1957, **45**, pp. 1249–1255

34 Hung, J.Y.: 'Feedback control with posicast', *IEEE Trans. Ind. Electron.*, 2003, **50**, pp. 94–99

35 Loh, P.C., Gajanayake, C.J., Vilathgamuwa, D.M., and Blaabjerg, F.: 'Evaluation of resonant damping techniques for Z-source current-type inverter'. Proc. IEEE, APEC, Dallas, TX, USA, 2006

36 Mattavelli, P., and Marafao, F.P.: 'Repetitive-based control for selective harmonic compensation in active power filters', *IEEE Trans. Ind. Electron.*, 2004, **51**, pp. 1018–1024

37 Bojoi, R.I., Griva, G., Bostan, V., Guerriero, M., Farina, F., and Profumo, F.: 'Current control strategy for power conditioners using sinusoidal signal integrators in synchronous reference frame', *IEEE Trans. Power Electron.*, 2005, **20**, pp. 1402–1412

38 Liserre, M., Teodorescu, R., and Blaabjerg, F.: 'Double harmonic control for three-phase systems with the use of resonant current controllers in a rotating frame', *IEE Trans. Power Electron.*, 2006, **21**, pp. 836–841

762

IEE Proc.-Electr. Power Appl., Vol. 153, No. 5, September 2006